

# Influence of surface structure and composition on neutralization of $^4\text{He}^+$ ions scattered from noble metals and alloy surfaces

D. Primetzhofer,<sup>1</sup> M. Spitz,<sup>1</sup> S. N. Markin,<sup>1</sup> E. Taglauer,<sup>2</sup> and P. Bauer<sup>1,\*</sup>

<sup>1</sup>*Institut für Experimentalphysik, Johannes Kepler Universität Linz, A-4040 Linz, Austria*

<sup>2</sup>*EURATOM Association, Max-Planck-Institut für Plasmaphysik, D-85748 Garching bei München, Germany*

(Received 17 June 2009; revised manuscript received 19 August 2009; published 25 September 2009)

Experiments to deduce ion fractions  $P^+$  of  $\text{He}^+$  ions scattered from  $\text{Ag}(110)$  and various  $\text{Au}$  surfaces in the low-energy ion scattering (LEIS) energy regime (0.6–9 keV) were performed by means of time-of-flight-LEIS. For  $\text{Au}$ ,  $P^+$  was measured for a  $\text{Au}(110)$   $1 \times 2$  reconstructed surface, a  $\text{Cu}_{0.5}\text{Au}_{0.5}(100)$  alloy crystal, and for polycrystalline  $\text{Au}$ . The well-ordered atomic structure of  $\text{Cu}_{0.5}\text{Au}_{0.5}(100)$  could be easily resolved. The results clearly indicate that  $P^+$  may depend strongly on the geometry and composition of the surface investigated. For  $\text{Au}(110)$  a remarkably high fraction of surviving ions from the surface layer was deduced from the experimental results.

DOI: [10.1103/PhysRevB.80.125425](https://doi.org/10.1103/PhysRevB.80.125425)

PACS number(s): 68.49.-h, 34.50.-s, 68.47.De, 68.49.Sf

## I. INTRODUCTION

In the low-energy ion scattering (LEIS) energy regime (0.5–10 keV) primary ions are typically very efficiently neutralized in the topmost layers of the scattering surface. If the signal of backscattered ions is detected by an electrostatic-analyzer-LEIS this strongly limits information depth and makes LEIS a very surface sensitive tool, whenever information on structure and composition of the outermost layers is of interest. In principle, a profound understanding of the different charge-exchange processes is available on a qualitative basis.<sup>1</sup> However, a quantitative prediction of the ion yield for a fixed geometry and a certain projectile and target element combination is not yet possible. Therefore, usually calibration by elemental standards is employed when quantitative analysis is needed.

Recent experiments by different groups showed independently that the neutralization efficiency for  $\text{He}^+$  scattered from elemental metal surfaces with different orientations may differ significantly.<sup>2–6</sup> For the experiments performed in grazing incidence an accurate theoretical model is available.<sup>7</sup> In LEIS, however, no crystal effect was expected since it was commonly accepted that the neutralization efficiency is a property of the combination of projectile and scattering center only.<sup>1</sup> However, some evidence for influence of the chemical environment and the trajectory has been reported in the literature.<sup>8–12</sup>

State-of-the-art description of charge exchange for noble gas ions on metallic surfaces distinguishes two types of processes: (i) Auger processes, which depend on the interaction time only and (ii) local collision-induced processes that are only active below a certain distance of projectile and target atom.

Auger neutralization (AN) along the trajectory is possible at any primary energy.<sup>13</sup> The neutralization rate— $dP^+/dt$ —depends on the Auger transition rate  $\Gamma_A$  via— $dP^+/dt = P^+\Gamma_A$ . Accordingly, surviving probabilities  $P_{\text{in}}^+$  and  $P_{\text{out}}^+$  for incoming and outgoing trajectories follow

$$P_j^+ = \exp\left[-\int_0^{\Delta t_j} \Delta^j \Gamma_A(z(t)) dt\right] = \exp[-\langle \Gamma_A \rangle \Delta t_j] \\ \approx \exp[-\langle \Gamma_A \rangle \Delta z_j / v_{\perp j}] \equiv \exp[-v_c / v_{\perp j}], \quad (1)$$

where  $j$  stands for *in* or *out*,  $\langle \Gamma_A \rangle$  denotes the transition rate averaged over the trajectory, and  $\Delta t$  is the time spent by the projectile in the region  $\Delta z$ , where neutralization processes occur. The characteristic velocity  $v_c$ , defined in Eq. (1), is a measure for neutralization efficiency. From Eq. (1) it is clear that AN scales with  $\Delta t$ , which is approximately equivalent to scaling with the velocity component  $v_{\perp}$  of the projectile normal to the surface.  $P_{\text{AN}}^+$  describes the fraction of projectiles that have survived surface scattering without being neutralized by AN and is given by  $P_{\text{AN}}^+ = P_{\text{in}}^+ P_{\text{out}}^+ = \exp[-\langle \Gamma_A \rangle (\Delta t_{\text{in}} + \Delta t_{\text{out}})] \approx \exp(-v_c / v_{\perp})$ , with the abbreviation  $1/v_{\perp} \equiv 1/v_{\perp \text{in}} + 1/v_{\perp \text{out}}$ .

Collision-induced processes, i.e., *collision-induced neutralization* and *reionization*, as already mentioned before, become possible for a minimum distance between projectile and scattering center smaller than a critical value  $R_{\text{min}}(E, \theta)$ .<sup>14–16</sup> In the collision between the projectile and a target atom, a minimum distance smaller than  $R_{\text{min}}$  is reached if for a fixed scattering angle  $\theta$  and the projectile energy  $E$  exceeds a certain threshold  $E_{\text{th}}$ . The specific value of  $E_{\text{th}}$  depends on the atomic species of the collision partners and on the scattering angle  $\theta$ , e.g., for  $\text{He}^+$  scattered from  $\text{Cu}$  and  $\theta = 129^\circ$ ,  $E_{\text{th}} = 2100$  eV.<sup>1</sup> Thus, the probabilities for the collision-induced processes,  $P_{\text{CIN}}$  and  $P_{\text{CIR}}$ , depend on  $E$  and  $\theta$  instead of  $v_{\perp}$ . Note, that at typical conditions  $P_{\text{CIN}} > P_{\text{CIR}}$  holds so that  $P^+ < P_{\text{AN}}^+$  in the reionization regime.

Recently, an additional nonlocal ionization process has been introduced; in an *Auger ionization* (AI) process two electrons are excited simultaneously, one from the projectile atomic level and one from the conduction band of the metal. AI, in contrast to AN requires a minimum kinetic energy of the projectile.<sup>7</sup> Therefore, this process will considerably contribute for high energies and may be relevant in the reionization regime only.

It is desirable to achieve more profound understanding of charge-exchange processes and of information depth, as required for applications, where quantitative information on surface composition is deduced exclusively from ion yields. In this respect many questions arise, e.g., whether charge-exchange processes are considerably influenced by the electronic structure of neighboring atoms or by the presence of electronic surface states.

This paper presents results of experiments performed for various noble metal and alloy crystals, i.e., Ag, Au, and  $\text{Cu}_{0.5}\text{Au}_{0.5}(100)$ . The main aim of this investigation was to find out whether the crystal effects observed for  $\text{He}^+$  and Cu are a unique property of this element or can also be observed for other materials. Furthermore, threshold energies for collision-induced processes were deduced and the trajectory dependence of  $P^+$  was investigated.

## II. EXPERIMENTAL SETUP

The experiments were performed using the time-of-flight (TOF-) LEIS setup ACOLISSA (Ref. 17) with a scattering angle  $\theta$  of  $129^\circ$  and a detector acceptance angle of  $0.92^\circ$ . The system is typically operated at a time resolution set to 10–25 ns corresponding to an energy resolution of 1–5 % for  $\text{He}^+$  ions at 3 keV. A post acceleration voltage can be applied along part of the flight path between sample and detector to separate backscattered ions from neutrals. The primary beam current is set between 25 and 100 nA in full beam mode, yielding 5–20 pA in the chopped beam mode, which makes TOF-LEIS virtually nondestructive. The beam current remains constant to within 10% after thermal equilibration ( $\sim 2$  h). At normal incidence, the beam spot on the sample was found to be smaller than 1 mm in diameter. From this the “safe” range of incident angles follows (angle of incidence  $\alpha < 65^\circ$ , with respect to the surface normal) ensuring that the whole irradiated spot is visible for the detector. The angular precision of the manipulator is  $\pm 0.1^\circ$  and  $\pm 0.2^\circ$  for polar and azimuth scans, respectively.

The samples were prepared by repetitive sputtering—annealing cycles, performed with 3 keV  $\text{Ar}^+$  ions and subsequent heating, typically to  $\sim 650$  K, depending on the sample. Surface purity was checked by Auger-electron spectroscopy and crystal structure of single crystals by low-energy electron diffraction.

Measurements were performed for Ag(110), Au(110) and  $\text{Cu}_{0.5}\text{Au}_{0.5}(100)$  single-crystal surfaces and polycrystalline Au.  $^4\text{He}^+$  ions with primary energies ranging from 0.6 to 9 keV were used as projectiles. For single crystals spectra were recorded in double alignment geometries, which suppress contributions from deeper layers due to channeling and blocking.<sup>18</sup> This allows determination of the ion fraction  $P^+$  from the areas of the surface peaks of neutrals and ions.<sup>5,19</sup> Ion fractions for polycrystalline samples were deduced from relative measurements by comparison to single crystals.<sup>20</sup>

## III. RESULTS AND DISCUSSION

Since the Au(110) surface usually exhibits a characteristic surface reconstruction additional experiments were performed on the unreconstructed Ag(110) surface. This provided the possibility of a direct comparison of the unreconstructed to the reconstructed (110) surface and a better understanding of how the scattering geometries influence the ion yield obtained.

Investigations for Ag(110) were performed for normal incidence. This surface offers the possibility to measure in double alignment geometry for different azimuth directions:

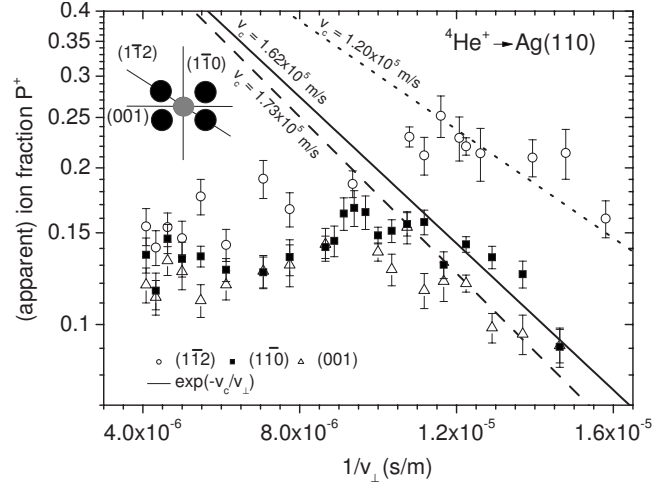


FIG. 1. Apparent ion fractions of  $^4\text{He}^+$  scattered from Ag(110) for normal incidence into different azimuth directions. The ion fraction for scattering exclusively by surface atoms is much higher than for the mixed contributions of first and second layer. Note that there is a small but distinct difference (10–20 % for  $E < E_{\text{th}}$ ) for the two different azimuth directions where second-layer contributions are included. The inset shows the azimuth directions for the surface investigated.

when the scattering plane is formed by the (110) and the  $(1\bar{1}2)$  directions, single scattering is possible exclusively from first-layer atoms; when the scattering plane contains the  $(1\bar{1}0)$  or the (001) azimuth directions, first and second layer contribute to the detected signal. In all these scattering geometries, first and second layer are equally illuminated by the primary beam and angular-dependent blocking of the second layer by first-layer atoms is responsible for the number of layers being visible for the detector. Note, that the outgoing trajectories of projectiles scattered from the second layer are very different for different azimuth directions: projectiles scattered perpendicularly to the densely packed rows pass the high-density electron cloud of first-layer atoms; if scattered in parallel, they only experience low electron densities (see sketch in Fig. 1). If two atomic layers contribute to the ion yield and the evaluation is performed straightforward from the ion and surface peak areas,  $A^+$  and  $A^0$ , respectively, the ion fraction obtained from the experimental quantities  $A^+$  and  $A^0$ ,  $P^+ \equiv A^+ / (A^+ + A^0)$  is only an apparent one. Consequently, if more than one layer contributes,  $P^+$  can only be approximated but not exactly described by Eq. (1). A perfect fit could be achieved by a sum of single exponential functions.

It is reasonable to expect the ion fraction for scattering from the first layer,  $P_1^+ = A_1^+ / (A_1^+ + A_1^0)$  to be higher than that for scattering from the second layer,  $P_2^+ = A_2^+ / (A_2^+ + A_2^0)$  and, consequently,  $P_1^+ \geq P^+$  and  $P_2^+ < P^+$ . Figure 1 shows the results for  $P_1^+$  [scattering plane formed by the surface normal and the  $(1\bar{1}2)$  azimuth direction] and  $P^+$  obtained for the (001) and  $(1\bar{1}0)$  azimuth scattering directions of Ag(110). If data are plotted as a function of  $1/v_{\perp}$  it is possible to fit the results in the subthreshold regime,  $E < E_{\text{th}}$ , for each geometry by a single exponential function. As a threshold energy for collision-induced processes,  $E_{\text{th}} \approx 1.25$  keV is obtained,

in good agreement with Ref. 15. In Fig. 1, comparison of open circles and full squares or open triangles reveals that  $P_1^+$  is almost twice of  $P^+$ . This is plausible since neutral yields are expected to be comparable,  $A_1^0 \approx A_2^0$  while the ion yields are not,  $A_1^+ \gg A_2^+$ . For the two different azimuth directions that include second-layer single scattered particles, a small but distinct difference in  $P^+$  can be found. The scattering plane that is intersected by the densely packed rows (001) exhibits lower ion fractions. Characteristic velocities  $v_c$  are found to be  $1.73 \times 10^5$  and  $1.62 \times 10^5$  m/s for the (001) and  $(1\bar{1}0)$  surface string directions, respectively. These results show that trajectory-dependent neutralization efficiencies are observed for projectiles backscattered in different azimuth direction by a single collision with an atom in the second layer. This effect is of special importance for very open surfaces such as fcc (110) where the ion yield contains significant contributions from the second layer, even for noble gas atoms as projectiles.

In order to quantify the ion fractions of individual layers, e.g., the second layer of Ag(110), the following model can be established: The intensities deduced from the surface peak areas  $A_0$  and  $A^+$  can be described by

$$A_0 = C_0 \sum_n^N c_n (1 - P_n^+) \quad (2)$$

and

$$A^+ = C^+ \sum_n^N c_n P_n^+, \quad (3)$$

where  $C_0$  and  $C^+$  denote experimental constants that include specific parameters such as primary beam current and detector efficiencies. In our setup,  $C_0$  and  $C^+$  are either identical or can easily be determined.<sup>17</sup> If  $N$  layers contribute to  $A_0$  and  $A^+$ , and all layers are equally illuminated by the primary beam and visible for the detector,  $c_n$  denotes the concentration of atoms per unit area in layer  $n$ . A necessary condition for the validity of Eqs. (2) and (3) is, that  $P_1^+$  does not exhibit any azimuth dependence. This is reasonable in LEIS since due to the large scattering angle only one surface atom—and not a surface string—is responsible for backscattering of the impinging ion. Another experimental justification will be presented later in this text.

Usually, for single crystals  $P^+$  is directly evaluated from  $A^+$  and  $A^0$ , as described above, correcting for different detection efficiencies  $\eta_+$  and  $\eta_0$  via

$$P^+ = \frac{1}{1 + \frac{A^0/\eta_0}{A^+/\eta_+}}. \quad (4)$$

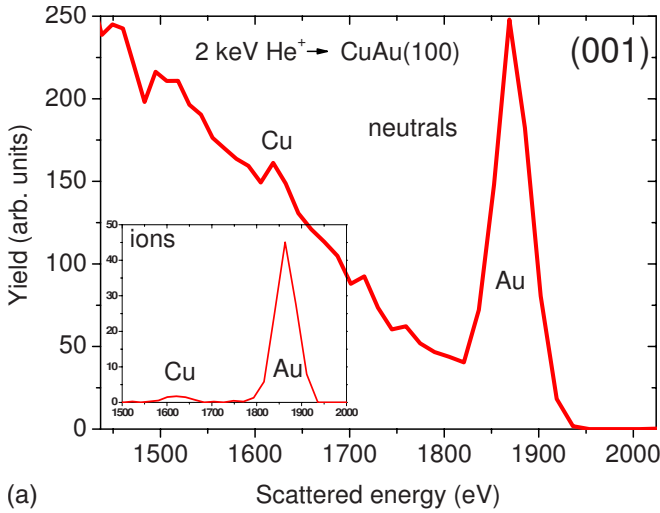
If  $N$  layers contribute, individual  $P_n^+$  values can be deduced from measurements of  $P^+$  in  $N$  nonequivalent geometries by use of Eqs. (2)–(4), as long as the coefficients  $c_n$  are known. In the present investigation of Ag(110),  $P_1^+$  is known from the experiments performed in  $(1\bar{1}2)$  azimuth direction and  $c_1 = c_2$ . This permits to evaluate  $P_2^+$  for both types of second-layer trajectories. E.g., for 1 keV He<sup>+</sup> ions,

$P_2^+ = 0.05$  is found in the  $(1\bar{1}0)$  azimuth direction while in the (001) direction  $P_2^+ = 0.01$  results. This shows that for subsurface atoms the ion signal may be strongly influenced by scattering geometry although in both cases it originates from single scattering only.

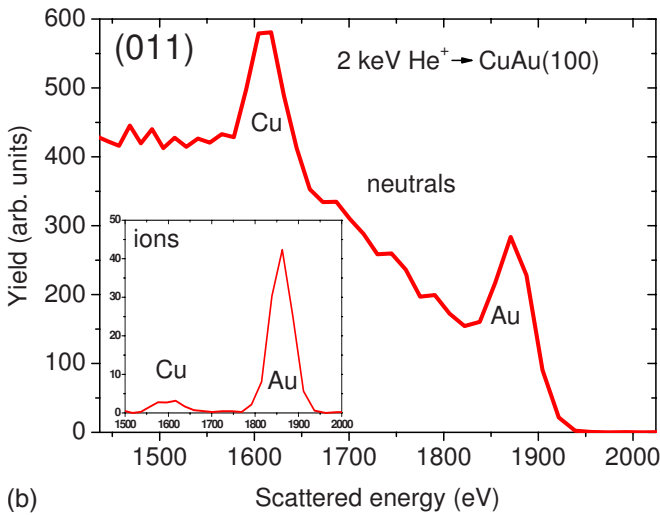
For the investigated surface, theoretical Auger rates  $\Gamma$  are available.<sup>21–23</sup> Linear interpolation of  $\Gamma$  and simulation of trajectories in the employed scattering geometry by the molecular-dynamics code KALYPSO (Ref. 24) yields a theoretical  $v_c$  of  $1.26 \times 10^5$  m/s, in excellent agreement with our experimental value of  $1.2 \times 10^5$  m/s.

With the insights gained from the study of neutralization at the unreconstructed Ag(110) surface, one can, as a next step, consider the more complex Au surfaces.  $\text{Cu}_{0.5}\text{Au}_{0.5}(100)$  is a crystal with extraordinary properties; ideally, the first layer is composed by Au atoms exclusively, followed by a Cu layer and again a Au layer, the atoms being arranged in an fcc lattice.<sup>25,26</sup> As typical for single crystals and double alignment geometry, clear surface peaks are observed for scattered neutrals and ions. Due to the substantial difference in mass, the surface peaks of Au and Cu can easily be resolved. This allows a direct evaluation of the ion fractions. Figures 2(a) and 2(b) present two energy-converted TOF spectra recorded for 2 keV He<sup>+</sup> ions at normal incidence and scattering into different azimuth directions, i.e., (001) and  $(0\bar{1}1)$ , respectively. In Fig. 2(a) one can observe a pronounced Au surface peak of neutrals accompanied by a very low background signal originating from multiple scattering. The inset shows the ion spectrum obtained by applying of a post acceleration voltage. For this azimuth direction the Cu atoms in the second layer are not directly visible for the detector. Therefore, virtually no contribution of Cu is found for the neutrals at the energy expected for backscattering in a single collision ( $k_{\text{Cu}}E_0 = 1628$  eV). Also, the ion signal for Cu is found to be very small, i.e. the ratio  $A_{\text{Au}}^+/A_{\text{Cu}}^+ \approx 30$ . Most probably,  $A_{\text{Cu}}^+$  may be attributed to surface defects and imperfect layer-separated ordering of Au and Cu. From this it can be estimated that in the surface layer about one out of ten Au atoms is replaced by Cu, taking the different scattering cross sections of Au and Cu into account.

In Fig. 2(b) the spectrum shape is remarkably different. For the chosen azimuth direction, i.e.,  $(0\bar{1}1)$  the second layer of Cu is completely visible, for the primary beam as well as for the detector. The Au surface peak looks qualitatively similar as in Fig. 2(a) and the peak areas  $A^+$  are equal in Figs. 2(a) and 2(b). For energies lower than expected for single scattering from Au, i.e., below  $k_{\text{Au}}E_0$ , a strong increase in the detected yield is observed. This can be attributed to enhanced multiple scattering from Au in this geometry and to small-angle scattering by Cu. At  $k_{\text{Cu}}E_0$  a large contribution of Cu to the backscattered neutrals is observed. Note, that  $A_{0,\text{Cu}} \approx A_{0,\text{Au}}$ , although the scattering cross section of Au is significantly higher ( $d\sigma_{\text{Au}}/d\sigma_{\text{Cu}} \approx 2.3$ ). This is attributed to very effective focusing of primary particles onto Cu atoms in the second layer. Also the ratio of the ion yields is changed, with  $A_{\text{Au}}^+/A_{\text{Cu}}^+ \approx 10$ . Note that  $A_{\text{Au}}^+$  does not change significantly. Consequently, an analysis of  $P_{\text{Au}}^+$  shows no azimuth dependence of the ion fraction. In terms of  $A_{\text{Cu}}^+$  it follows that in Fig. 2(b) the ion yield is increased by a factor of about 3,



(a)



(b)

FIG. 2. (Color online) *Energy-converted TOF spectra obtained for 2 keV  $^4\text{He}^+$  ions scattered from  $\text{Cu}_{0.5}\text{Au}_{0.5}(100)$  with post acceleration voltage applied. The inset shows the ion spectrum. (a) Normal incidence and  $\phi=0^\circ$ —azimuth (001). (b) Normal incidence and  $\phi=45^\circ$ —azimuth (011). In (a) almost no Cu contribution is visible and the ion signal ratio  $A_{\text{Au}}^+/A_{\text{Cu}}^+$  is around 30. In (b) elevated background contributions are observed at all energies displayed. Additionally, a clear Cu surface peak appears. The ion signal ratio  $A_{\text{Au}}^+/A_{\text{Cu}}^+$  is around 10.*

due to contributions from Cu in the second layer. This is of importance for surface composition analysis; a naïve evaluation of elemental surface concentrations from the ion yields in Fig. 2(b), a Cu concentration of  $\sim 25\%$  would erroneously result.

For all further investigations the ion fraction of Au in  $\text{Cu}_{0.5}\text{Au}_{0.5}(100)$  was determined only for the geometry corresponding to Fig. 2(a). Figure 3 shows the resulting  $P_{\text{Au}}^+$  for  $^4\text{He}^+$  scattered from  $\text{Cu}_{0.5}\text{Au}_{0.5}(100)$ , Au(110), and polycrystalline Au in the energy range 0.6–2 keV. For all surfaces investigated one single reionization threshold is found,  $E_{\text{th}} \approx 1$  keV, in good agreement with (Ref. 15). Furthermore, this shows that the  $E_{\text{th}}$  is indeed a property of scatterer and projectile atom only, without any influence of the matrix. For energies below  $E_{\text{th}}$  the ion fraction  $P^+$  can be described by

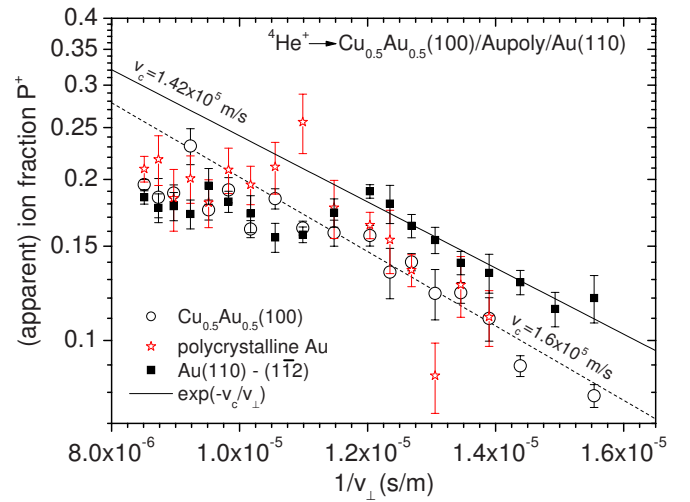


FIG. 3. (Color online) *(Apparent) ion fractions obtained for  $^4\text{He}^+$  ions with energies between 0.6 and 2 keV scattered in double alignment geometries from  $\text{Cu}_{0.5}\text{Au}_{0.5}(100)$  and  $\text{Au}(110)$  and for normal incidence from polycrystalline Au. The ion fractions for  $\text{Au}_{\text{poly}}$  and  $\text{Cu}_{0.5}\text{Au}_{0.5}(100)$  are equal within statistical uncertainties.  $P^+$  for Au(110) shows a distinct difference for energies below the threshold for reionization  $E_{\text{th}}$  which was experimentally determined to be 1 keV.*

Eq. (1). Note, that there is no statistically significant difference in  $P^+$  for  $\text{He}^+$  scattered from Au in  $\text{Cu}_{0.5}\text{Au}_{0.5}(100)$  or from polycrystalline Au (open circles and asterisks, respectively), i.e. all data can be fitted by a single exponential function with  $v_c = 1.60 \times 10^5$  m/s. For the  $(1\bar{1}2)$  azimuth direction of Au(110), higher  $P^+$  values (full squares in Fig. 3) are obtained than for the other surfaces at energies below  $E_{\text{th}}$ . The corresponding  $v_c$  is found to be  $1.42 \times 10^5$  m/s. This again can be attributed to a crystal effect. In contrast, in the reionization regime  $P^+$  turns out to be equal or lower than for the other surfaces investigated.

Since Au(110) is a reconstructed surface, it is not possible to limit the single-scattering contributions to the outermost atomic layer with the experimental setup used, as it was the case for Ag(110). Au(110) exhibits a  $1 \times 2$  “missing row” reconstruction at the conditions of the presented experiments.<sup>27,28</sup> In the scattering geometry presented in Fig. 3, i.e., normal incidence and  $(1\bar{1}2)$  azimuth, first and second layer are equally contributing to the yield of particles backscattered in a single collision. Since the orientation of the surface is different to  $\text{Cu}_{0.5}\text{Au}_{0.5}(100)$ , no significant focusing of primary particles onto the second layer is observed. Again, of course there is a significant difference in the survival probability of ions for scattering from each layer and the obtained ion fraction is only an apparent one. Thus, it is clear, that for  $^4\text{He}^+$  and the first layer of Au(110)  $P_1^+$  will be significantly higher than  $P^+$  and a pronounced crystal effect has to be expected.

In contrast to Ag(110), for Au(110) and normal incidence of  $\text{He}^+$  it is possible to measure in two distinct azimuth directions with different numbers of atoms from the second layer,  $c_2$ , contributing to the backscattered yield. For azimuth (001),  $c_2 = 2c_1$ ; for azimuth  $(1\bar{1}2)$ ,  $c_2 = c_1$ . Figure 4 presents

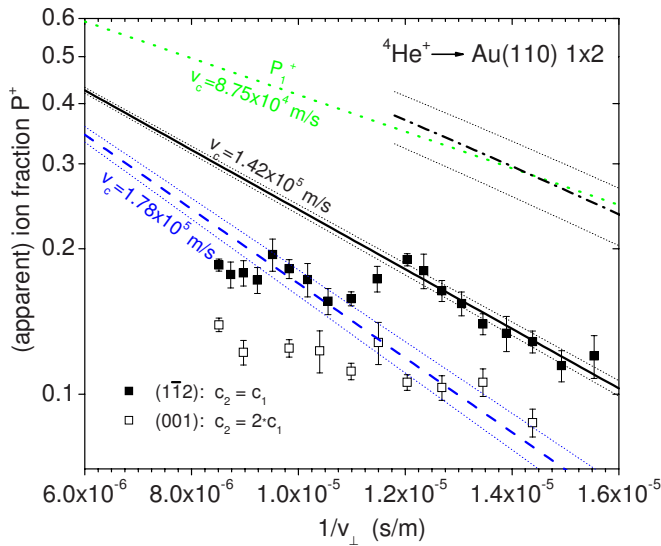


FIG. 4. (Color online) Measured apparent ion fractions for  ${}^4\text{He}^+$  ions and primary energies of 0.6–2 keV scattered for various azimuth orientations from the Au(110)  $1 \times 2$  reconstructed surface (full and open squares). Fits to the data in the Auger regime are shown with the corresponding characteristic velocity  $v_c$  and their uncertainties (black and blue full and dashed lines). The figure also shows the deduced ion fraction  $P_1^+$  of the first layer and its uncertainty resulting from the uncertainty of measured data (black dash-dotted line). Since this line is no single exponential,  $P_1^+$  is obtained as a fit according to Eq. (1) (green dotted line), with an extraordinarily low characteristic velocity ( $v_c = 8.75 \times 10^4$  m/s).

experimental results for these two different azimuth scattering planes. The pronounced difference in  $P^+$  already indicates—as expected—that  $P_1^+$  will be significantly higher than  $P_2^+$  and any directly measured apparent  $P^+$ . If now the calculation is performed including the uncertainties in the  $v_c$  values as outlined before, one obtains  $P_1^+$  (green dotted line in Fig. 4). Note, that the results of this evaluation (black dash-dotted line) are not exactly described by Eq. (1). Finally,  $P_1^+$  is obtained as a fit of a single exponential [see Eq. (1)].

The results show that  $P_1^+$  is extraordinarily high for the reconstructed Au(110) surface compared to  $\text{Cu}_{0.5}\text{Au}_{0.5}(100)$  or polycrystalline Au; an increase of almost a factor of 2 is observed. The characteristic velocity  $v_c$  that fits the deduced values of  $P_1^+$  is found to be  $8.75 \times 10^4$  m/s.

This result clearly indicates, that in Au(110) the electronic structure of the outermost layer is very different from that of deeper layers or other Au surfaces. Similar conclusions have been drawn from previous investigations by different techniques.<sup>29,30</sup> Furthermore, it was reported that surface states present in other Au surfaces are missing in Au(110).<sup>31</sup>

#### IV. CONCLUSIONS

The neutralization behavior of and Au surface atoms embedded in different matrices was experimentally investigated. Threshold energies  $E_{\text{th}}$  for collision-induced charge exchange were determined. For a certain combination of projectile and target atom,  $E_{\text{th}}$  was found to be equal for pure metal and alloy crystals. This confirms the local character of collision-induced processes. Trajectory-dependent apparent ion fractions for scattering in different azimuth directions from Ag(110) surface atoms were observed. This is attributed to different electron densities along the trajectories. Scattering from the second layer can significantly contribute to the obtained ion yield.

Also for Au, strong crystal effects can be observed. Whereas Au in  $\text{Cu}_{0.5}\text{Au}_{0.5}$  and polycrystalline Au exhibits similar neutralization behavior, Au(110) showed extraordinarily high ion fractions for the first layer. These findings were deduced from experimental results recorded in distinct geometries. The first layer of Au(110) behaves completely different in comparison to other Au surfaces, as observed in other investigations. Pronounced subsurface contributions to the ion yield have been observed. Thus, it was shown that a profound understanding of charge-exchange processes and of information depth is demanded, whenever quantitative information on surface composition is deduced exclusively from ion yields. Finally, the manifold results reported proof that TOF-LEIS is a very powerful tool for probing electronic and structural properties of surfaces.

#### ACKNOWLEDGMENTS

This work was partly supported by the Austrian Science Fund (FWF) under Contract No. P16469-N08. Inspiring discussions with Carmina Monreal are gratefully acknowledged. D. Primetzhofer acknowledges financial support by the Austrian Academy of Science.

\*Corresponding author; peter.bauer@jku.at

<sup>1</sup>H. H. Brongersma, M. Draxler, M. de Ridder, and P. Bauer, Surf. Sci. Rep. **62**, 63 (2007).

<sup>2</sup>Yu. Bandurin, V. A. Esaulov, L. Guillemot, and R. C. Monreal, Phys. Rev. Lett. **92**, 017601 (2004).

<sup>3</sup>Yu. Bandurin, V. A. Esaulov, L. Guillemot, and R. C. Monreal, Phys. Status Solidi B **241**, 2367 (2004).

<sup>4</sup>S. Wethekam, D. Valdes, R. C. Monreal, and H. Winter, Phys. Rev. B **78**, 075423 (2008).

<sup>5</sup>D. Primetzhofer, S. N. Markin, E. Taglauer, and P. Bauer, Phys. Rev. Lett. **100**, 213201 (2008).

<sup>6</sup>D. Primetzhofer, S. N. Markin, J. I. Juaristi, E. Taglauer, and P. Bauer, Nucl. Instrum. Methods Phys. Res. B **267**, 624 (2009).

<sup>7</sup>S. Wethekam, D. Valdes, R. C. Monreal, and H. Winter, Phys. Rev. B **78**, 033105 (2008).

<sup>8</sup>D. J. Godfrey and D. P. Woodruff, Surf. Sci. **105**, 438 (1981).

<sup>9</sup>D. J. Godfrey and D. P. Woodruff, Surf. Sci. **105**, 459 (1981).

<sup>10</sup>E. Taglauer, W. Englert, W. Heiland, and D. P. Jackson, Phys.

- Rev. Lett. **45**, 740 (1980).
- <sup>11</sup>M. Beckschulte and E. Taglauer, Nucl. Instrum. Methods Phys. Res. B **78**, 29 (1993).
- <sup>12</sup>J. P. Jacobs, S. Reijme, R. J. M. Elfrink, S. N. Mikhailov, M. Wuttig, and H. H. Brongersma, J. Vac. Sci. Technol. A **12**, 2308 (1994).
- <sup>13</sup>H. D. Hagstrum, Phys. Rev. **96**, 336 (1954).
- <sup>14</sup>R. Souda, M. Aono, C. Oshima, S. Otani, and Y. Ishizawa, Surf. Sci. **150**, L59 (1985).
- <sup>15</sup>T. M. Thomas, H. Neumann, A. W. Czanderna, and J. R. Pitts, Surf. Sci. **175**, L737 (1986).
- <sup>16</sup>N. P. Wang, E. A. Garcia, R. Monreal, F. Flores, E. C. Goldberg, H. H. Brongersma, and P. Bauer, Phys. Rev. A **64**, 012901 (2001).
- <sup>17</sup>M. Draxler, S. N. Markin, S. N. Ermolov, K. Schmid, C. Hesch, R. Gruber, A. Poschacher, M. Bergsmann, and P. Bauer, Vacuum **73**, 39 (2004).
- <sup>18</sup>Th. Fauster, Vacuum **38**, 129 (1988).
- <sup>19</sup>D. Primetzhofer, S. N. Markin, J. E. Valdés, E. Taglauer, R. Beikler, and P. Bauer, Nucl. Instrum. Methods Phys. Res. B **258**, 36 (2007).
- <sup>20</sup>S. N. Markin, D. Primetzhofer, J. E. Valdés, E. Taglauer, and P. Bauer, Nucl. Instr. and Meth. B **258**, 18 (2007).
- <sup>21</sup>D. Valdés, J. M. Blanco, V. A. Esaulov, and R. C. Monreal, Phys. Rev. Lett. **97**, 047601 (2006).
- <sup>22</sup>D. Valdés, R. C. Monreal, and V. A. Esaulov, Nucl. Instrum. Methods Phys. Res. B **256**, 6 (2007).
- <sup>23</sup>D. Valdés, J. M. Blanco, V. A. Esaulov, and R. C. Monreal, Phys. Rev. B **75**, 165404 (2007).
- <sup>24</sup>M. A. Karolewski, Nucl. Instrum. Methods Phys. Res. B **230**, 402 (2005).
- <sup>25</sup>Y. Teraoka, Surf. Sci. **242**, 113 (1991).
- <sup>26</sup>E. Taglauer and R. Beikler, Vacuum **73**, 9 (2004).
- <sup>27</sup>W. Moritz and D. Wolf, Surf. Sci. **163**, L655 (1985).
- <sup>28</sup>T. Gritsch, D. Coulman, R. J. Behm, and G. Ertl, Surf. Sci. **257**, 297 (1991).
- <sup>29</sup>K. Stahrenberg, T. Herrmann, N. Esser, W. Richter, S. V. Hoffmann, and P. Hofmann, Phys. Rev. B **65**, 035407 (2001).
- <sup>30</sup>C. J. Fall, N. Binggeli, and A. Baldereschi, Phys. Rev. B **61**, 8489 (2000).
- <sup>31</sup>P. Cortona, M. G. Dondi, D. Cvetko, A. Lausi, A. Morgante, K. C. Price, and F. Tommasini, Phys. Rev. B **47**, 6705 (1993).